pressure, turbulent premixed CH_4/air flame (Reynolds's number approximately 5000 based on the tube diameter of 1.3 cm), stabilized by means of a thin, coaxial CH_4/air diffusion flame.

A number of digital pictures of the flow patterns were recorded using different NO seed levels (premixed into the fuel/air flow), different excitation wavelengths, and different fields of view.

Theory

Assuming weak excitation by a broadband laser source, the fluorescence signal S_F can be related to the NO total number density N_{NO} via the equation:[4]

$$S_F = CI\frac{A_{21}}{A_{21}+Q}f_p(T)B_{12}N_{NO} \quad (1)$$

where C is a constant that includes geometrical and efficiency factors, I is the laser spectral irradiance, $A_{21}/(A_{21}+Q)$ is the photon yield or Stern-Vollmer factor, Q is the electronic quenching rate, A_{21} and B_{12} are the Einstein coefficients for the transition, and $f_p(T)$ is the fraction of NO in the state being pumped.

The proportionality factor between the fluorescence signal and the total NO number density can be regarded as a constant provided that the product of the Stern-Vollmer factor and the population factor does not vary significantly throughout the flowfield being studied. This can often be accomplished by choosing a molecular transition with an appropriate temperature dependence in the population factor. Alternatively, a transition may be selected so that there is a nearly constant relation between S_F and NO mole fraction. If a measurement of temperature is the goal (for example in a flow with fixed NO mole fraction) a transition with a strong, known temperature dependence may be selected.

Two different laser wavelengths ($\lambda = 225.598$ and 224.526 nm) were chosen corresponding to the $R_1(16)$ line and the $Q_1(35)$ line of the $A^2\Sigma^+(v=0) \leftarrow X^2\Pi_{1/2}(v=0)$ band of NO. The fluorescence signal arising from excitation of the $R_1(16)$ line is temperature insensitive (estimated change of $\pm 10\%$ in $f_p A_{21}/(A_{21}+Q)$ between 500 and 2000 K), so that the measured fluorescence intensity distribution is expected to be proportional to the NO number density distribution. Similarly, excitation of the $Q_1(35)$ line provides a signal proportional to the NO mole fraction in the temperature range 1100-2400 K.

Results

Figure 2 is a single-shot digital picture of the fluorescence signal generated in the plane of illumination of the laser, above the stoichiometric CH_4/air flat flame burner. The laser was tuned to the $Q_1(35)$ line of NO providing 0.9 mJ/pulse with a bandwidth of approximately 0.5 cm^{-1} and pulse duration of about 8 ns. The NO seeding level was 1900 ppm in the inlet gas stream. The fluorescence intensity is seen to be nearly constant in the inner part of the flame, as expected, since no mixing has occurred with the surrounding air. The local variations in signal that are observed in this core region are thought to be due to pixel-to-pixel variations in responsivity and shot noise. At the edges of the flame, diffusion and mixing reduce the NO mole fraction, resulting in reduced fluorescence. The large-scale structures produced at the unstable boundary between the hot flame gases and the cool surrounding air are clearly visualized in these records, indicating the potential of this diagnostic technique for quantitative studies of such phenomena.

Figure 3 shows digital pictures of the NO fluorescence in a stoichiometric, premixed CH_4/air turbulent flame, with the laser tuned to the $Q_1(35)$ line. NO is premixed in the inlet flow with a mole fraction of 3800 ppm. Background emission (due to the luminosity of the flame) was eliminated by subtraction of two frames with the laser on and off, respectively. Owing to the much higher Reynolds number of this flame, the NO signal corresponds more nearly to that of a jet with constant mole fraction in the inner core independent of combustion reactions. The different character of the mixing regions at the boundaries of the flame gases, relative to the low-speed flame shown in Fig. 2 is clearly apparent.

Conclusions

Planar laser-induced flourescence (PLIF) with a Reticon array imaging system has been used to visualize NO in combustion flowfields with submillimeter and submicrosecond resolution. The NO was seeded to laminar and turbulent CH_4/air flames. The lowest seed level used was 350 ppm premixed with the fuel/air flows. NO levels down to 30 ppm in the outer parts of the flames were resolved on a single-shot basis. Using improved collection optics, NO mole fractions smaller than 10 ppm should be detectable.

The seeding of flows with NO overcomes some of the disadvantages of previously used seed materials such as iodine[5] (useful only in cold flows) and sodium[6] (requires heating, and uniform seeding is difficult to achieve). NO is relatively stable at temperatures up to 2000 K in many combustion environments, and therefore seems well suited for use in visualizing combustion as well as cold flows.

By choosing different NO molecular transitions it is possible to provide fluorescence distributions which vary in their sensitivity to temperature. It should therefore be possible to visualize temperature, mole fraction, and number density by pumping appropriate molecular transitions. This capability should be of importance in studies of mixing processes. Moreover the technique is sufficiently sensitive to be useful in studies of NO chemical kinetics in combustion flows.

Acknowledgments

This work was supported by the Air Force Office of Scientific Research under contract F-49620-80-C-0091. K. Knapp acknowledges the Deutsche Forschungsgemeinschaft, West Germany, for a fellowship during his stay at Stanford University.

References

[1] Kychakoff, G., Howe, R. D., Hanson, R. K., and McDaniel, J. C., *Applied Optics*, Vol. 21, 1982, p. 3225.

[2] Dyer, M. J. and Crosley, D. R., *Optics Letters*, Vol. 7, 1982, p. 382.

[3] Kychakoff, G., Howe, R. D., Hanson, R K., and Knapp, K., AIAA Paper 83-0405, Reno, Nev., Jan. 1983.

[4] Bechtel, J. H. and Chraplyvy, A. R., *Proceedings of IEEE*, Vol. 70, 1982, p. 658.

[5] McDaniel, J. C., Baganoff, D., and Byer, R. L., *Physics of Fluids*, Vol. 25, 1982, p. 1105.

[6] Kychakoff, G. and Hanson, R. K., Paper 81-50, Western States Section/The Combustion Institute, Phoenix, Ariz., Oct. 1981.

A Uniformly Valid Asymptotic Solution for Unsteady Subresonant Flow Through Supersonic Cascades

O. O. Bendiksen*
Princeton University, Princeton, New Jersey

Introduction

LOW-FREQUENCY approximations of unsteady flow through supersonic cascades with a subsonic leading-edge

Submitted Jan. 20, 1983; revision received April 1, 1983.

*Assistant Professor, Department of Mechanical and Aerospace Engineering.

locus have been obtained by several investigators.[1-4] These solutions have a singularity at an interblade phase angle $\sigma=0$, arising from the collapse of the superresonant region to the point $k=\sigma=0$ as the reduced frequency $k\to 0$. It should be noted that for all $k>0$, the singular point $\sigma=0$ lies not in the superresonant but in the subresonant region. The purpose of this Note is to show that a uniformly valid low-frequency expansion for the subresonant region can be obtained by suitably redefining the underlying limit process $k\to 0$.

Low-Frequency Approximations

Consider an infinite two-dimensional cascade executing simple harmonic motion. In a coordinate system at rest with respect to the cascade, and with the flow at infinity aligned with the x axis (Fig. 1; Ref. 5), the space part of the linearized potential equation governing the flow is

$$\beta^2\frac{\partial^2\Psi}{\partial\bar{x}^2}-\frac{\partial^2\Psi}{\partial\bar{y}^2}+2ikM^2\frac{\partial\Psi}{\partial\bar{x}}-k^2M^2\Psi=0 \tag{1}$$

The notation is the same as in Ref. 5: $k=\omega b/U$, $\bar{x}=x/b$, $\bar{y}=y/b$, $b=$ semichord, $\beta^2=M^2-1$, $M=$ Mach number, etc.

Now let $k=\epsilon\ll 1$ and consider asymptotic expansions representing approximate solutions of Eq. (1), based on the limit process $\epsilon=k\to 0$; remaining parameters fixed. It is then clear that the term $k^2M^2\Psi$ in Eq. (1) is of second order in $\epsilon=k$, and can therefore be neglected without affecting the validity of a first-order solution (the *superresonant* region is an exception). Using the same procedure as in Refs. 4 and 5, the approximate boundary-value problem for the entire cascade, consistent to first order in $\epsilon=k$, can be recast in the form of the following dual integral equations between the upwash $\bar{v}_0(\bar{x})$ and pressure jump $[\bar{p}_0(\bar{x})]$ across the reference (zeroth) blade and its extension $-\infty<\bar{x}<\infty$, $\bar{y}=0$:

$$\bar{v}_0(\bar{x})=\frac{i\beta}{2}\int_{-\infty}^{\infty}G_1(\tau+\bar{k}M)F_0(\tau+\bar{k}M)e^{i\bar{x}\tau}\,d\tau \tag{2}$$

$$[\bar{p}_0(\bar{x})]=\int_{-\infty}^{\infty}F_0(\tau+\bar{k}M)e^{i\bar{x}\tau}\,d\tau \tag{3}$$

where $\bar{v}_0(\bar{x})$ is known from the flow tangency condition for $|\bar{x}|<1$, and $[\bar{p}_0(\bar{x})]=0$ for $|\bar{x}|>1$. Here

$$G_1(\tau)=\frac{\tau}{\tau-\bar{k}/M}G_\infty(\tau) \tag{4}$$

$$G_\infty(\tau)=\frac{\sin(\bar{s}_2\beta\tau)}{\cos(\bar{s}_2\beta\tau)-\cos(\Omega-\bar{s}_1\tau)}$$
$$=-i\sum_{m=0}^{\infty}\exp[im(\Omega-\kappa_1\tau)]-i\sum_{m=1}^{\infty}\exp[-im(\Omega-\kappa_2\tau)] \tag{5}$$

where $\bar{k}=kM/\beta^2$, $\Omega=\sigma+\bar{s}_1\bar{k}M$, $\bar{s}_1=\bar{s}\sin\theta$, $\bar{s}_2=\bar{s}\cos\theta$, $\bar{s}=s/b$, $s=$ blade spacing along the leading-edge locus, $\theta=$ stagger angle, $\kappa_1=\bar{s}_1+\beta\bar{s}_2$, $\kappa_2=\bar{s}_1-\beta\bar{s}_2$. Unless otherwise noted, an overbar signifies a nondimensionalized quantity: lengths with respect to semichord b, velocities with respect to flow velocity U at infinity, and pressures with respect to ρ_0U^2. To ensure the existence of certain integrals and the convergence of infinite series such as Eq. (5), the reduced frequency k is assumed to have a small negative imaginary part, $k=k_1-ik_2$, $0<k_2\ll 1$, and the limit $k_2\to 0^+$ is implied throughout. Also, in Eq. (2) and subsequent Cauchy type integrals, the Cauchy principal value is implied.

Now $G_\infty(\tau)$ is the reduced kernel associated with the quasistatic problem, or the steady problem if $\Omega=0$, for which an exact solution has been obtained[4]:

$$F_0(\tau+\bar{k}M)=\sum_{n=0}^{\infty}a_nj_n(\tau) \tag{6}$$

where, for the case $\kappa_1,\ \kappa_2>2$,

$$a_n=(-i)^n\frac{(2n+1)}{\pi\beta}\int_{-1}^{1}\bar{v}_0(\bar{x})P_n(\bar{x})\,d\bar{x} \tag{7}$$

and j_n is the spherical Bessel function of the first kind of order n, and P_n is the Legendre polynomial of degree n. It now will be shown that the solution of the present problem is also of the form given by Eq. (6), which already satisfies Eq. (3) identically.[5] When Eq. (6) is substituted into the upwash integral equation, Eq. (2), one obtains

$$\bar{v}_0(\bar{x})=\sum_{n=0}^{\infty}a_n\phi_n(\bar{x}) \tag{8}$$

where

$$\phi_n(\bar{x})=\frac{i\beta}{2}\int_{-\infty}^{\infty}G_1(\tau+\bar{k}M)j_n(\tau)e^{i\bar{x}\tau}\,d\tau\quad(|\bar{x}|<1) \tag{9}$$

For the case $\kappa_1>2$, $\kappa_2>2$, corresponding to a cascade with no Mach wave reflections, the integral in Eq. (9) is[4]

$$\frac{2}{\pi\beta i^n}\phi_n(\bar{x})=P_n(\bar{x})+i\frac{k}{\beta^2}e^{-ik\bar{x}}\int_{-1}^{\bar{x}}P_n(u)e^{iku}\,du$$
$$-2i^{1-n}\frac{k}{\beta^2}j_n(-k)e^{-ik\bar{x}}S(k,\sigma) \tag{10}$$

where

$$S(k,\sigma)=-\sum_{m=1}^{\infty}e^{-im\Omega^*}=\frac{1}{1-e^{i\Omega^*}}=\frac{1}{2}+\frac{i}{2}\cot\frac{\Omega^*}{2} \tag{11}$$

and $\Omega^*=\Omega-\kappa_2\bar{k}/M=\sigma+k(\bar{s}_1+\bar{s}_2/\beta)$. Here the fact that $\mathrm{Im}\Omega^*<0$ has been used in summing the infinite series S. The singularities of S consist of an infinite set of simple poles at $\Omega^*=2\pi\nu$; $\nu=0,\ \pm1,\ \pm2,\ldots$, which in the limit $k_2\to 0^+$ approach the real σ axis from above. Only one of these singularities lies in the range of interblade phase angles $0\le\sigma<2\pi$, and can be shown to be inside the superresonant region. For fixed k, the superresonant region is defined as $\sigma_{r1}<\sigma<\sigma_{r2}$, where the resonance points σ_{r1} and σ_{r2} are the two solutions between 0 and 2π of the equation

$$\Omega=\sigma+\bar{s}_1\bar{k}M=2\pi\nu\pm\bar{k}\bar{d}\qquad\nu=0,\pm1,\pm2,\ldots \tag{12}$$

and $\bar{d}=\sqrt{\kappa_1\kappa_2}$.

It is now clear that any limit process expansion based on $k\to 0$, σ fixed, will move the singularity at $\sigma=-k(\bar{s}_1+\bar{s}_2/\beta)$ to $\sigma=0$, as observed in previously obtained solutions.[1-4] However, if one redefines the underlying limit process as $k\to 0$, Ω^* (and all remaining variables *except* σ) fixed, then it is possible to obtain uniformly valid approximations for the entire subresonant region. Note that in this limit, the precise locations of the singularities of $S(k,\sigma)$ are preserved, and therefore remain within the superresonant regime throughout the limit process. It is then readily shown that S is of order $1/k$ as the end (resonance) points of the subresonant region are approached. Since $j_n(-k)\sim\mathcal{O}(k^n)$ as $k\to 0$, it is clear that the last term in Eq. (10) is, at worst, $\mathcal{O}(k^n)$ close to the resonance points and $\mathcal{O}(k^{n+1})$ sufficiently away from these points.

For cascade geometries where Mach wave reflections occur, the shape functions defined by Eq. (9) will have discontinuities in $\bar{x}$ where leading- or trailing-edge waves from adjacent blades impinge. These discontinuities can be removed by redefining the shape functions by explicitly accounting for the reflections by the method used in Ref. 4. The modified shape functions $\phi^*(\bar{x})$ complete to $\mathcal{O}(k)$ are then

$$\frac{2}{\pi\beta}\phi_0^*(\bar{x})=P_0(\bar{x})+i\frac{k}{\beta^2}[(\bar{x}+1)-2(1-ik\bar{x})S^*(\Omega^*)] \tag{13}$$

$$\frac{2}{\pi\beta i}\phi_1^*(\bar{x}) = P_1(\bar{x}) + \frac{ik}{\beta^2}\left[\frac{1}{2}(\bar{x}^2-1) - \frac{2}{3}ikS^*(\Omega^*)\right] \quad (14)$$

$$\frac{2}{\pi\beta i^n}\phi_n^*(\bar{x}) = P_n(\bar{x}) + i\frac{k}{\beta^2}\int_{-1}^{\bar{x}} P_n(u)\,du \quad (n>1) \quad (15)$$

where $S^*(\Omega^*)=S(\Omega^*)\kappa_2/2$ for $0<\kappa_2\le 2$ and $S^*(\Omega^*)=S(\Omega^*)$ for $\kappa_2>2$. As $k=\epsilon\to 0, \phi_n^*(\bar{x})\to \text{const}\cdot P_n(\bar{x})+\mathcal{O}(\epsilon)$ uniformly in $\bar{x}$ for σ in the subresonant regime. Since the Legendre polynomials are complete and form an orthogonal basis on $[-1,1]$, a solution to $\mathcal{O}(\epsilon=k)$ of Eq. (8) is readily found. If S can be assumed of order one, i.e., if σ is well inside the subresonant region, then such a solution can be determined by standard perturbation techniques. By repeated application of $\epsilon\to 0$, Ω^* fixed, one finds that the successive orders of the coefficients a_n are given by Eq. (7), with $\bar{v}_0(\bar{x})$ suitably defined. For bending-torsion oscillations, the result is

$$a_0 = \frac{2\bar{v}_{0b}}{\pi\beta}\left\{1-\frac{ik}{\beta^2}[1-2S^*(\Omega^*)]\right\} - \frac{2\alpha_0}{\pi\beta}\left\{1-iak-\frac{ik}{\beta^2}[1-2S^*(\Omega^*)]\right\} \quad (16)$$

$$a_1 = \frac{2k}{\pi\beta^3}[\bar{v}_{0b}+(\beta^2-1)\alpha_0] \quad (17)$$

where $\bar{v}_{0b}$ is the bending velocity amplitude $(=-ikh_0)$, positive up; α_0 the torsional displacement amplitude about axis $\bar{x}=a$, positive clockwise. The lift (positive up) and moment (about midchord, positive clockwise) amplitudes are[4]:

$$L_0 = -2\pi\rho_0 U^2 b F_0(\bar{k}M) \quad (18)$$

$$M_{0_{mc}} = 2\pi i\rho_0 U^2 b^2 F_0'(\bar{k}M) \quad (19)$$

In the absence of Mach wave reflections $F_0(\bar{k}M)=a_0$ and $F_0'(\bar{k}M)=a_1/3$, but for the general case all a_n are involved. For Verdon's cascade A,[6] corresponding to one reflection of upward propagating waves, the following expressions are obtained:

$$F_0(\bar{k}M) = a_0 - \left(1-\frac{\kappa_2}{2}\right)\left[a_0+i\frac{\kappa_2}{2}a_1\right]\exp[-i(\sigma+\bar{k}M\beta\bar{s}_2)] \quad (20)$$

$$F_0'(\bar{k}M) = \frac{a_1}{3} + \left(1-\frac{\kappa_2}{2}\right)\left[(\kappa_2^2+2\kappa_2-2)\frac{a_1}{6} - i\frac{\kappa_2}{2}a_0\right] \times \exp[-i(\sigma+\bar{k}M\beta\bar{s}_2)] \quad (21)$$

Expressions corresponding to other Mach wave reflection patterns can be found in Ref. 4.

On substituting $\Omega^*\to\sigma$ and expanding $\exp[-i(\sigma+\bar{k}M\beta\bar{s}_2)]\simeq(1-i\bar{k}M\beta\bar{s}_2+\ldots)\exp(-i\sigma)$, the solution given by Eqs. (16-21) can be shown to agree with expansions obtained by Nagashima and Whitehead.[2] Also, the results for torsional oscillations are in agreement with those of Kurosaka,[1] while his results for bending oscillations are based on displacements rather than velocity and therefore correspond to the $\mathcal{O}(1)$ terms in the present solution.

The solution given by Eqs. (16 and 17) presupposes that S (or S^*) is of order one, and therefore cannot be expected to be valid to $\mathcal{O}(\epsilon=k)$ close to the resonance points. In fact, since the order of the term $\epsilon S^*(\epsilon,\sigma)$ varies continuously between $\mathcal{O}(\epsilon)\le\mathcal{O}(\epsilon S^*)\le\mathcal{O}(1)$ as σ sweeps through the subresonant region, ϕ_n^* is not simply a power series in ϵ, nor can the solution be assumed to be of this form. A uniformly valid solution can be obtained by solving Eq. (8) directly, recognizing that the shape functions ϕ_n^* are uniformly valid to $\mathcal{O}(\epsilon)$ and asymptotic to the Legendgre polynomials. For the bending-torsion case previously considered, this yields

$$a_0 = \frac{2[\bar{v}_{0b}-\alpha_0(1-iak)]}{\pi\beta\{1+i(k/\beta^2)[1-2S^*(\Omega^*)]\}} \quad (22)$$

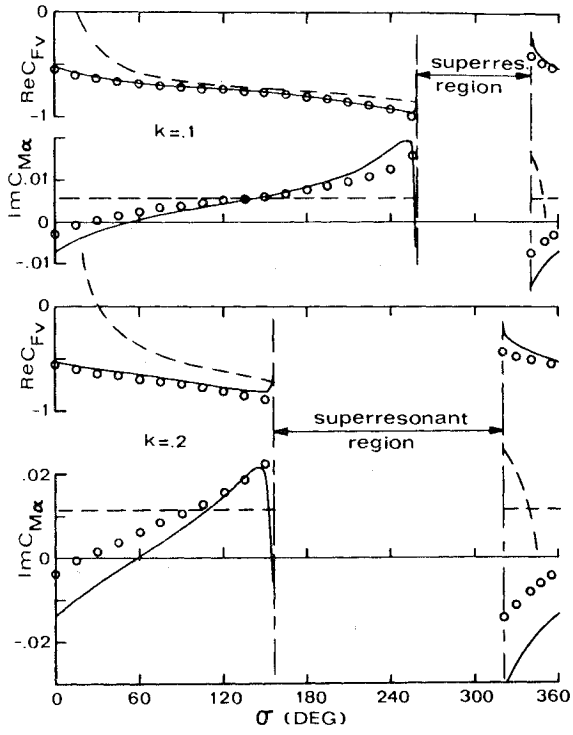

Fig. 1 Comparison of low-frequency approximations to lift and moment coefficients $C_{Fv}=-F_0(\bar{k}M)/\bar{v}_{0b}$ and $C_{M\alpha}=iF_0'/(2\alpha_0)$ due to bending and torsional oscillations, respectively: ○ present approximation; – – – nonuniform approximations[2,4]; ——full unsteady solution.[4] $\bar{s}_2=2.5$, $\theta=60$ deg, $M=1.3$, $a=0$.

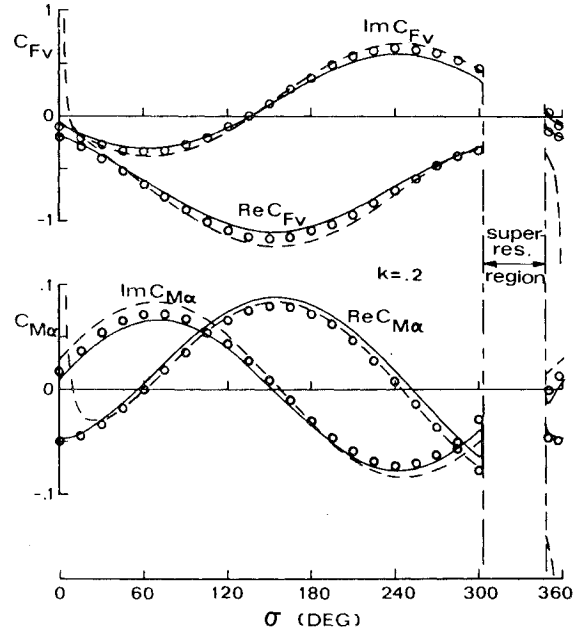

Fig. 2 Comparison of low-frequency approximations of C_{Fv} and $C_{M\alpha}$ for Verdon's cascade A. Legend same as in Fig. 1. $\bar{s}_2=0.8$, $\theta=59.5$ deg, $M=1.345$, $a=0$.

$$a_1 = -\frac{k}{\beta^2} a_0 [1 + 2ikS^*(\Omega^*)] - \frac{2k\alpha_0}{\pi\beta} \quad (23)$$

When $S^*(\Omega^*)$ is $\mathcal{O}(1)$, application of the binomial theorem recovers Eqs.(16) and (17) to $\mathcal{O}(\epsilon = k)$.

Numerical Examples and Conclusions

Figures 1 and 2 illustrate typical results for two cascade configurations: a low-solidity cascade with no Mach wave reflections (Fig. 1), and Verdon's cascade A (Fig. 2). Unsteady lift and moment amplitudes are calculated by the uniformly valid formulas, Eqs. (22) and (23), and Eqs. (18-21), and compared to previously obtained (nonuniform) approximations as well as the full unsteady solution. Note that the nonuniform approximation is actually quite good for cascade A, except for the range $\sigma_{r_2} \leq \sigma \leq 360 + 30$ deg. It breaks down surprisingly quickly, however, for the low-solidity cascade, for which the improvements obtained by using the uniformly valid approximation are most apparent.

References

[1]Kurosaka, M., "On the Unsteady Supersonic Cascade with a Subsonic Leading Edge—An Exact First Order Theory: Parts 1 and 2," *ASME Journal of Engineering for Power*, Vol. 96, Jan. 1974, pp. 13-31.

[2]Nagashima, T. and Whitehead, D. S., "Linearized Supersonic Unsteady Flow in Cascades," Great Britain Aeronautical Research Council R&M 3811, 1978.

[3]Strada, J. A., Chadwick, W. R., and Platzer, M. F., "Aeroelastic Stability Analysis of Supersonic Cascades," ASME Paper 78-GT-151, April 1978.

[4]Bendiksen, O. O., "Coupled Bending-Torsion Flutter in Cascades with Applications to Fan and Compressor Blades," Ph.D. Dissertation, Mechanics and Structures Dept., Univ. of California, Los Angeles, March 1980; also available as UCLA Rept. ENG-8072, July 1980.

[5]Bendiksen, O. and Friedmann, P., "Bending-Torsion Flutter in Supersonic Cascade," *AIAA Journal*, Vol. 19, June 1981, pp. 774-781.

[6]Verdon, J. M., "Further Developments in the Aerodynamic Analysis of Unsteady Supersonic Cascades, Parts 1 and 2," *ASME Journal of Engineering for Power*, Vol. 99, Oct. 1977, pp. 509-525.

Rule of Forbidden Signals in a Two-Dimensional Supersonic Compressor Cascade

David C. Prince Jr.*
General Electric Company, Cincinnati, Ohio

Introduction

THIS Note reviews some two-dimensional supersonic compressor cascade data that demonstrate obedience to the "Rule of Forbidden Signals"[1] over substantial portions of both suction and pressure surfaces. It also shows that two-dimensional method of characteristics (MOC) analysis without boundary-layer allowance predicts the surface pressures in the zone of silence extremely well. The Note also reported on progress at refining previous MOC analyses for more realistic representation of experimental shock structures.

Received Oct. 15, 1982; revision received April 15, 1983.

*Consulting Engineer, Aircraft Engine Business Group. Associate Fellow AIAA.

There seems to be some confusion in the literature over what role the Rule of Forbidden Signals[1] ought to play in analysis and experiments on transonic and supersonic flows in compressor cascades. As early as 1973, some experience showing that supersonic pressure surface pressures in compressor rotors responded to throttling was reported in Ref. 2. This experience seemed to violate forbidden signals. It was well known before that time that the "pressure ratio vs flow at constant speed" characteristic for a supersonic compressor rotor at even moderate supersonic Mach numbers was essentially vertical. Signal propagation upstream all the way through the rotor really was forbidden. Reference 2 also reported on some early efforts at analytical modeling of flow in supersonic compressor cascades, using both time-marching and MOC approaches. As long as MOC modeling was strictly two dimensinal and inviscid, it was clearly bound by the restrictions of forbidden signals. A specification on axial variation of laminar thickness could be used to control the exit Mach number level. This type of analysis assumed that only one laminar thickness specification could be allowed for all back pressures, which precluded any approach to the experimental results in zone of silence regions.

Boundary-layer behavior has received considerable attention as an area for investigation in the search for explanation of compressor and cascade flow observations. There is, of course, no doubt that suction surface boundary layers must interact with the incident leading-edge shock across the cascade or rotor passage inlet. It is however, pressure surface phenomena that are most conspicuous examples of apparent forbidden signal violations.

York and Woodard[3] used an MOC approach to analytical modeling of supersonic compressor cascade flow. They were able to show encouraging correspondence between their predicted wave patterns and schlieren photographs of a cascade test. They also showed good agreement between measured and predicted suction surface pressures, without dependence on boundary-layer analysis to support the agreement. They did not discuss the implications of their work relative to forbidden signals.

Experimental Data with Inviscid Analysis

The experimental results used by York and Woodard were presented in much greater detail by Fleeter et al.[4] Figure 1 is a composite of schlieren photographs presented in Ref. 4 for fixed Mach number and varying back pressure. It is easy to see that the wave pattern in the leading-edge region and through most of the cascade passage is independent of back pressure over a substantial range. Unfortunately, some loss of periodicity appears at the higher back pressures (which are still below the 2.16 design value). Figure 2 demonstrates the influence of the downstream pressure on the surface pressure distributions. The pressures are plotted against projected position on the airfoil surfaces. Tic marks on the airfoils indicate the locations of the pressure sensors. Approximate locations for the downstream limit to the zone of silence are determined by points where an increase in the downstream pressure has produced a change in the local pressure. Above a downstream pressure ratio of 1.9, the zone of silence boundary jumps forward from the passage exit to the passage inlet. The forward 50% of the suction surface remains in the zone of silence throughout the range of the data in the figure.

Also shown on Fig. 2 for comparison are an inviscid MOC wave pattern for downstream pressure ratio of 1.58 and predicted surface pressure distributions for pressure ratios 1.58 and 1.21 (predicted shock waves and pressure distributions are indicated by heavy dashed lines). The techniques for this analysis were outlined in Ref. 5. 1.58 is the highest pressure ratio at which the inviscid flow downstream of the reflected trailing-edge shock remains supersonic. (Note on this figure that the flow has considered shock losses but not viscous flow losses.) The correspondence between the